Absence of SO(4) quantum criticality in Dirac semimetals at two-loop order

Max Uetrecht, Igor F. Herbut, Emmanuel Stamou, and Michael M. Scherer

¹Fakultät Physik, Technische Universität Dortmund, D-44221 Dortmund, Germany ²Department of Physics, Simon Fraser University, Burnaby, British Columbia, Canada V5A 1S6 ³Institut für Theoretische Physik III, Ruhr-Universität Bochum, D-44801 Bochum, Germany (Dated: August 25, 2023)

Evidence for relativistic quantum criticality of antiferromagnetism and superconductivity in twodimensional Dirac fermion systems has been found in large-scale quantum Monte Carlo simulations. However, the corresponding (2+1)-dimensional Gross-Neveu-Yukawa field theory with $N_f=2$ four-component Dirac fermions coupled to two triplets of order parameters does not exhibit a renormalization group fixed point at one-loop order. Instead, the theory only features a critical point for a large or very small fractional number of fermion flavors N_f , which disappears for a broad range of flavor numbers around the physical case, $N_f = 2$, due to fixed-point annihilation. This raises the question on how to explain the observed scaling collapse in the quantum Monte Carlo data. Here, we extend previous renormalization-group analyses by studying a generalized model at two-loop order in $4-\epsilon$ spacetime dimensions. We determine the ϵ correction to the upper and lower critical flavor numbers for the fixed-point annihilation and find that they both go towards the physical case $N_f = 2$. However, this only happens very slowly, such that an extrapolation to $\epsilon = 1$ still suggests the absence of criticality in 2+1 dimensions. Thereby, we consolidate the finding that the continuum field theory does not feature a stable renormalization-group fixed point and no true quantum criticality would be expected for the considered system. We briefly discuss a possible reconciliation in terms of a complex conformal field theory. Further, we also explore the fixed-point structure in an enlarged theory space and identify a candidate stable fixed-point solution.

I. INTRODUCTION

The quantum critical behavior of two-dimensional gapless Dirac electrons undergoing a transition into an ordered phase is characterized by the generalized Gross–Neveu universality classes, ^{1–4} which are distinct from the conventional universality classes known from statistical models. The advent of Dirac materials, ^{5,6} has boosted the interest in these universality classes ^{7–20} which may even come within experimental reach, when electronic interactions are strong enough to induce symmetry-breaking phase transitions as, e.g., observed in magicangle graphene at charge neutrality. ^{21–24}

The critical exponents of the Gross–Neveu universality classes depend on the symmetries of the order-parameter field and the number of Dirac fermions. For example, for the case of the chiral Ising model, their precise computation has recently been pushed forward through progress in the conformal bootstrap, $^{25-27}$, quantum Monte Carlo simulations $^{28-30}$ and renormalization group methods, $^{31-33}$ and a satisfactory agreement between the estimates for the exponents across different theoretical approaches has already been achieved.

For other cases, however, whereas the different theoretical methods confirm the existence of a distinct Gross–Neveu quantum critical point between the Diracsemimetal phase and an ordered state, the quantitative agreement between them remains more elusive. An important example of these is the chiral Heisenberg universality class that describes the transition towards an antiferromagnetic state in graphene, ^{33–38} see the recent discussion presented in Ref. [4]. More work is required to achieve consensus on the precise value of the critical exponents. Despite such quantitative differences, these findings support the general picture that the critical behavior near a continuous (quantum) phase transition is not governed by the specifics of a microscopic model but that it can be captured in terms of a universal continuum field theory. This universal theory shares the symmetries, dimensionality, and field content of the microscopic model as, e.g., required for a quantum Monte Carlo simulation.

Interestingly, a recent quantum Monte Carlo study explored the transition of a system with two four-component Dirac fermions going from a semimetallic into a massive phase including a Néel state and a superconductor-CDW state.³⁹ The quantum Monte Carlo data reported in Ref. [39] supports a scaling collapse indicative of a quantum critical point in the $SO(3)\times SO(3) \simeq SO(4)$ – symmetric field theory. In contrast, a subsequent renormalization-group study of the corresponding continuum field theory could not identify a stable fixed point of the model,⁴⁰ suggesting the absence of critical behavior without additional fine-tuning, at least on the one-loop level studied in Ref. [40].

These incompatible findings call for reconciliation and options for a resolution are the following: i) The lattice model studied in Ref. [39] corresponds to a different continuum field theory, e.g., one with additional topological terms compatible with the symmetries. ii) The one-loop renormalization group misses the underlying fixed point, which could be recovered at higher-loop orders. iii) The transition observed in the lattice model is of weak first order merely mimicking critical behavior.

TABLE I. Field content of $4-\epsilon$ dimensional theory in Eq. (5) and its transformation properties under the global SU(2)_A × SU(2)_B symmetry and the Lorentz group. n labels the number of Dirac-bidoublet fermions, and we have suppressed their SU(2)_A × SU(2)_B indices for brevity.

	$\mathrm{SU}(2)_{\mathrm{A}}$	$\mathrm{SU}(2)_{\mathrm{B}}$	Lorentz
Ψ_n	2	2	$\left(\frac{1}{2},0\right) + \left(0,\frac{1}{2}\right)$
a_i	3	_	_
b_j	_	3	_

All of these options hint towards an interesting underlying physical mechanism, e.g., the question about possible topological contributions according to i) or the similarity to the deconfined quantum phase transitions^{41–44} of option iii). Option ii) would have a certain similarity to the Banks–Zaks fixed point^{45–47} in non-abelian gauge theories, suggesting that the current scenario could shed some light on this related phenomenon in quantum chromodynamics. In the present work, we aim at clarifying option ii) on the two-loop level.

The rest of the paper is organized as follows. In the next section, we present the continuum (2+1)-dimensional Gross–Neveu–Yukawa field theory with two adjoint order parameters coupled to fermions,⁴⁰ and present its analytic continuation to $d=4-\epsilon$ (see Appendix A for a detailed derivation). Then, in Section III, we elaborate on our automated two-loop renormalization procedure and explicitly state our results for the two-loop β -functions and anomalous dimensions in $d=4-\epsilon$. In Section IV, we perform a fixed-point analysis, both in the symmetric subspace of the model studied by quantum Monte Carlo calculations for a generalized number of fermion flavors N_f , and in the full, unconstrained parameter space for $N_f=2$, which corresponds to graphene. Finally, in Section V, we discuss and summarize our results.

II. GROSS-NEVEU-YUKAWA MODEL WITH TWO ORDER PARAMETERS

The model we study is given in Refs. [39] and [40] and describes a Gross-Neveu-Yukawa field theory in d=2+1 Euclidean spacetime dimensions with an eight-component complex fermion field ψ that is coupled to two triplets of order parameters. These order parameters are denoted in the following as $a_i t_i$ and $b_j t_j$, with i, j = 1, 2, 3 and where a_i and b_j are real scalar fields with $t_k = \frac{\sigma_k}{2}$, where σ_k denote the usual Pauli matrices satisfying the Clifford algebra $\{\sigma_k, \sigma_l\} = 2\delta_{kl} \mathbb{1}$. The scalars transform as (1, 0) + (0, 1) under the global SO(4) \simeq SO(3) \times SO(3) symmetry group, which is locally isomorphic to the product of two distinct SU(2) groups, i.e., SU(2)_A \times SU(2)_B.

Using the projective $SU(2) \simeq SO(3)$ isomorphism we couple the fermionic field to the order parameters. The

corresponding d=2+1 Lagrangian in $\it Euclidean$ spacetime reads

$$\mathcal{L}_{d=2+1} = \mathcal{L}_{\psi} + \mathcal{L}_{ab} + \mathcal{L}_{\psi ab}, \qquad (1)$$

with fermionic, bosonic, and Yukawa-type contributions⁴⁸

$$\mathcal{L}_{\psi} = \psi^{\dagger} \partial_{\tau} \psi + \psi^{\dagger} \Big[\mathbb{1}_{4 \times 4} \otimes \sum_{k=1}^{2} \sigma_{k} \left(-i \frac{\partial}{\partial x_{k}} \right) \Big] \psi , \quad (2)$$

$$\mathcal{L}_{ab} = \frac{1}{2} \Big[(\partial_{\mu} a_{i}) (\partial^{\mu} a_{i}) + (\partial_{\mu} b_{j}) (\partial^{\mu} b_{j}) \Big] \\
- \frac{r_{a}}{2} (a_{i} a_{i}) - \frac{r_{b}}{2} (b_{j} b_{j}) \\
- \frac{\lambda_{a}}{8} (a_{i} a_{i})^{2} - \frac{\lambda_{b}}{8} (b_{j} b_{j})^{2} - \frac{\lambda_{ab}}{4} (a_{i} a_{i}) (b_{j} b_{j}) , \quad (3)$$

$$\mathcal{L}_{\psi ab} = -\psi^{\dagger} \Big[g_{a} (a_{i} t_{i}) \otimes \mathbb{1}_{2 \times 2} + g_{b} \mathbb{1}_{2 \times 2} \otimes (b_{j} t_{j}) \Big] \otimes \beta \psi , \quad (4)$$

where $\beta = \sigma_3$ is hermitian and anticommutes with σ_1 and σ_2 . In Ref. [40] the eight-component fermion field ψ is split into $N_f = 2$ four-component fermion fields. Note that compared to Ref. [40] we have rescaled the fields and couplings by constant factors.

The Yukawa couplings, $g_{a/b}$, and the quartic couplings, $\lambda_{a/b/ab}$, are not marginal in d=3, thus, we cannot perform standard perturbation-theory computations in d=3. However, if the theory admits a continuation in $d=4-\epsilon$ dimensions, where the couplings are marginal, and has perturbative fixed points for small ϵ , it is amenable to computations within the framework of ϵ -expansion. ⁴⁹ This can be used to provide quantitative extrapolations of fixed-point dynamics in the d=3 theory, which is the case for the model in Eq. (1).

To this end, it is essential to formulate the theory such that it can be continuously interpolated from d=4 to d=3 spacetime dimensions. In Appendix A, we present in detail how to continue the theory of Eq. (1) in $d=4-\epsilon$. Here, we present the final result of the continuation in Minkowskian spacetime. It features the scalars, a_i and b_j , whose continuation is straightforward, and an N_{Ψ} number of four-component Dirac fields, Ψ_n , which transform as bidoublets under the global symmetry group SU(2)_A×SU(2)_B. In Table I we summarize the field content of the theory and its transformation properties.

The corresponding $d = 4 - \epsilon$ Lagrangian in Minkowskian spacetime with N_{Ψ} number of four-component Diracbidoublet fermions, Ψ_n , reads

$$\mathcal{L} = \overline{\Psi}_n i \partial_\mu \gamma^\mu \Psi_n + \frac{1}{2} \left[(\partial_\mu a_i) \left(\partial^\mu a_i \right) + (\partial_\mu b_j) \left(\partial^\mu b_j \right) \right]$$

$$- \frac{r_a}{2} (a_i a_i) - \frac{r_b}{2} (b_j b_j)$$

$$- \frac{\lambda_a}{8} \left(a_i a_i \right)^2 - \frac{\lambda_b}{8} \left(b_j b_j \right)^2 - \frac{\lambda_{ab}}{4} (a_i a_i) (b_j b_j)$$

$$- g_a \overline{\Psi}_n \left(a_i t_i \right) \Psi_n - g_b \overline{\Psi}_n \left(b_j t_j \right) \Psi_n , \tag{5}$$

with $\mu = 0, 1, 2, 3$ and γ^{μ} the 4×4 Dirac matrices. The Lagrangian is manifestly Lorentz invariant. For brevity,

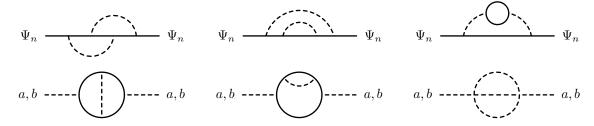


FIG. 1. Example Feynman diagrams entering the computation of the fermionic (upper) and bosonic (lower) two-point functions at the two-loop level. Such diagrams contribute to the respective field renormalization constants Z_{Ψ} and $Z_{a/b}$.

we have kept the contractions of the $SU(2)_{A/B}$ indices implicit.

The steps required to derive the Lagrangian in Eq. (5) starting from the d=3 Euclidean Lagrangian in Eq. (1) are presented in detail in Appendix A. First, we repackage the eight-component fermion field, ψ , of the d=3Lagrangian into a single two-component Dirac-bidoublet fermion, $\Psi_{aA}^{d=3}$. Next, we make Lorentz invariance manifest by re-expressing the β - and σ -matrices in terms of Euclidean gamma matrices, and subsequently rotating to Minskowski where $\{\gamma^0, \gamma^1, \gamma^2\} = \{\beta, -\beta\sigma_1, -\beta\sigma_2\}$ with $\{\gamma^{\mu}, \gamma^{\nu}\} = 2g^{\mu\nu}$ and $g^{\mu\nu} = \text{diag}(+, -, -)$. The final step is to continue the theory from d=3 to d=4. In the former, Dirac fermions are complex two-component fields, whereas in the latter they are complex four-component fields, which implies that the naïve continuation of the d=3 Lagrangian to d=4 contains twice as many fermionic degrees of freedom. Therefore, in order to describe graphene, i.e., a single $\Psi_{aA}^{d=3}$, from the $4-\epsilon$ Lagrangian in Eq. (5) within the ϵ -expansion we must set $N_{\Psi} = 1/2$. This corresponds to $N_f = 4N_{\Psi}$ in the definition of N_f from Ref. [40].

III. RENORMALIZATION GROUP AT TWO-LOOP LEVEL

We compute the β functions and anomalous dimensions of the d-dimensional theory in Eq. (5) by the standard renormalization procedure: fields and couplings are renormalized and the value of their renormalization constants are extracted from the divergent terms of appropriate Green's functions. The renormalization constants then fix the β functions and anomalous dimensions of the theory. We work within dimensional regularization in $d=4-\epsilon$ spacetime dimensions and employ the mass-independent $\overline{\text{MS}}$ renormalization scheme. In this section, we introduce our notation, briefly describe the relevant computations for determining the Renormalization Group Equations (RGEs) at the two-loop level, and present our results.

Specifically, we renormalize the bare fields and couplings

in Eq. (5) (denoted with the superscript "(0)" below) via

$$\begin{split} \Psi_{n}^{(0)} &= Z_{\Psi}^{1/2} \Psi_{n} \,, & a_{i}^{(0)} &= Z_{a}^{1/2} a_{i} \,, \\ b_{j}^{(0)} &= Z_{b}^{1/2} b_{j} \,, & r_{a,b}^{(0)} &= r_{a,b} + \delta r_{a,b} \,, \\ g_{a}^{(0)} &= \mu^{\epsilon/2} Z_{g_{a}} g_{a} \,, & g_{b}^{(0)} &= \mu^{\epsilon/2} Z_{g_{b}} g_{b} \,, \\ \lambda_{a,b,ab}^{(0)} &= \mu^{\epsilon} \left(\lambda_{a,b,ab} + \delta \lambda_{a,b,ab} \right) \,. \end{split}$$
(6)

Note that all fields and the Yukawa couplings, $g_{a/b}$, are multiplicatively renormalized, while the order parameters, $r_{a,b}$, and the quartics, $\lambda_{a,b,ab}$, must be additively renormalized. The independence of the bare coupling on the artificial $\overline{\rm MS}$ scale μ defines the RGEs in the standard way.

We have determined all the above renormalization constants up to two-loop accuracy by explicit computation and renormalization of offshell, one-particle-irreducible Green's functions. The fermion and scalar field renormalization constants are extracted from the fermion and scalar two-point functions, respectively; in Figure 1 we show representative two-loop diagrams for the fermion two-point function, and for the scalar two-point function. The scalar two-point function additionally fixes the additive renormalization constant for the order parameters, i.e., $\delta r_{a,b}$. To determine the renormalization of the Yukawa couplings, $Z_{g_{a,b}}$, we renormalize the fermion-fermion-scalar three-point functions (see Figure 2 for some representative two-loop diagrams) and to determine the renormalization of quartics, $\delta \lambda_{a,b,ab}$, we renormalize the four-scalar four-point functions (see Figure 3).

To extract the renormalization constants from the UV poles of offshell, one-particle irreducible Green's functions it suffices to compute those in terms of an expansion in small external momenta (and masses). The expansion leads to scaleless loop-integrals that vanish in dimensional regularization due to the cancellation of IR and UV divergences⁵⁰. We thus employ the method of Infrared Rearrangement (IRA),⁵¹ which introduces an artificial mass $m_{\rm IRA}$ that serves as an IR regulator. This enables us to extract the UV divergences from computing "simple" two-loop tadpole diagrams⁵² that depend on a single mass, i.e., $m_{\rm IRA}$. The recursion relations and the corresponding master integrals are given in Ref. [53]. Even though intermediate steps of the computation can depend on the artificial mass $m_{\rm IRA}$ – counterterms proportional to

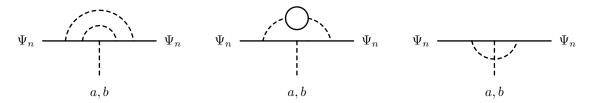


FIG. 2. Example Feynman diagrams entering the computation of the fermion–fermion–scalar three-point functions at the two-loop level relevant for extracting the renormalization constants of the Yukawa couplings, $Z_{g_{a/b}}$.

 m_{IRA}^2 may be required to cancel all subdivergences – the final renormalization constants do not depend on m_{IRA} . For further details, we refer to the original discussion in Ref. [51]. In our case, the only such "IRA counterterm" that can and does enter the computation corresponds to scalar mass terms, i.e., $m_{\mathrm{IRA}}^2 a_i a_i$ and $m_{\mathrm{IRA}}^2 b_j b_j$.

The two-loop calculation involves hundreds of different diagrams. We thus make use of the automated setup MaRTIn,⁵⁴ which employs QGRAF⁵⁵ for the diagram generation and FORM⁵⁶ routines to evaluate the amplitudes. MaRTIn performs the IRA, the tensor reduction to scalar integrals, the reduction to master integrals, and the Dirac algebra. We performed all computations by using our own implementation of the model in Eq. (5) and by extending MaRTIn with a custom routine to perform the $SU(2)_{A,B}$ algebra. All one-loop results agree with the correspondig calculations in Ref. [40]. As an indepenent check of the explicit two-loop computation, we have obtained the twoloop RGEs using the toolkit ARGES⁵⁷ and find an exact agreement. An additional check of the computation is provided by available two-loop β -functions of the chiral and the statistical Heisenberg model, ³³ as these models are subsectors of our model with two triplet order parameters.

Having obtained the renormalization constants in Eq. (6), we readily obtain the β -functions and anomalous dimensions of the theory from the independence of the bare quantities on the scale μ . The continuum RGEs given below are directly related to the ones in the Wilsonian Renormalization Group (WRG) by substituting $\frac{d}{d\log\mu} \to -\frac{d}{d\log b}$, with b controlling the inclusion of IR modes in the momentum-shell integration of the WRG. In what follows, we collect the resulting RGEs for the $d=4-\epsilon$ theory at two-loop accuracy. Note that in the corresponding RGEs in Ref. [40] the quantity N_f denotes the number of four-component fermion fields, which is related to the number of Dirac bidoublets, N_{Ψ} , via $N_f=4N_{\Psi}$ (cf. Section II).

Yukawa β -functions

In the $d = 4 - \epsilon$ theory, the β -functions for the Yukawa couplings, $g_{a,b}$, are defined as

$$\beta_{g_X}(\epsilon) \equiv \frac{dg_X^2}{d\log\mu} = -\epsilon g_X^2 + \sum_{i=1}^{\infty} \left(\frac{1}{16\pi^2}\right)^n \beta_{g_X}^{(n)}, \quad (7)$$

with $X \in \{a, b\}$. We find for the one- and two-loop terms

$$\beta_{g_a}^{(1)} = \frac{1 + 8N_{\Psi}}{2} g_a^4 + \frac{9}{2} g_a^2 g_b^2 , \qquad (8)$$

$$\beta_{g_a}^{(2)} = \frac{47 - 192N_{\Psi}}{32} g_a^6 - \frac{33 + 120N_{\Psi}}{16} g_a^4 g_b^2$$

$$- \frac{177 + 336N_{\Psi}}{32} g_a^2 g_b^4 + \frac{3}{2} \lambda_{ab}^2 g_a^2 - 9 g_a^2 g_b^2 \lambda_{ab}$$

$$- 5 g_a^4 \lambda_a + \frac{5}{2} g_a^2 \lambda_a^2 , \qquad (9)$$

and analogously $\beta_{g_b}(\epsilon) = \{\beta_{g_a}(\epsilon) \text{ with } a \leftrightarrow b\}.$

Quartic β -functions

Similarly, the β -functions for the quartics are defined as

$$\beta_{\lambda_X}(\epsilon) \equiv \frac{d\lambda_X}{d\log\mu} = -\epsilon\lambda_X + \sum_{i=1}^{\infty} \left(\frac{1}{16\pi^2}\right)^n \beta_{\lambda_X}^{(n)}, \quad (10)$$

with $X \in \{a, b, ab\}$. For λ_a we find at one- and two-loop level

$$\beta_{\lambda_{a}}^{(1)} = -4N_{\Psi}g_{a}^{4} + 8N_{\Psi}g_{a}^{2}\lambda_{a} + 11\lambda_{a}^{2} + 3\lambda_{ab}^{2}, \qquad (11)$$

$$\beta_{\lambda_{a}}^{(2)} = +8N_{\Psi}g_{a}^{6} + 24N_{\Psi}g_{a}^{4}g_{b}^{2} - 3N_{\Psi}g_{a}^{4}\lambda_{a} - 15N_{\Psi}g_{a}^{2}g_{b}^{2}\lambda_{a} + 12N_{\Psi}g_{a}^{2}g_{b}^{2}\lambda_{ab} - 44N_{\Psi}g_{a}^{2}\lambda_{a}^{2} - 12N_{\Psi}g_{b}^{2}\lambda_{ab}^{2} - 69\lambda_{a}^{3} - 15\lambda_{a}\lambda_{ab}^{2} - 12\lambda_{ab}^{3}, \qquad (12)$$

and by analogy $\beta_{\lambda_b}(\epsilon) = \{\beta_{\lambda_a}(\epsilon) \text{ with } a \leftrightarrow b\}$. For the λ_{ab} β -function we instead find

$$\beta_{\lambda_{ab}}^{(1)} = -12N_{\Psi}g_{a}^{2}g_{b}^{2} + 4N_{\Psi}(g_{a}^{2} + g_{b}^{2})\lambda_{ab} + 5(\lambda_{a} + \lambda_{b})\lambda_{ab} + 4\lambda_{ab}^{2},$$
(13)
$$\beta_{\lambda_{ab}}^{(2)} = +32N_{\Psi}(g_{a}^{4}g_{b}^{2} + g_{a}^{2}g_{b}^{4}) + 10N_{\Psi}g_{a}^{2}g_{b}^{2}(\lambda_{a} + \lambda_{b}) + N_{\Psi}g_{a}^{2}g_{b}^{2}\lambda_{ab} - \frac{11}{2}N_{\Psi}(g_{a}^{4} + g_{b}^{4})\lambda_{ab} - 8N_{\Psi}(g_{a}^{2} + g_{b}^{2})\lambda_{ab}^{2} - 20N_{\Psi}(g_{a}^{2}\lambda_{a} + g_{b}^{2}\lambda_{b})\lambda_{ab} - 30(\lambda_{a} + \lambda_{b})\lambda_{ab}^{2} - \frac{25}{2}(\lambda_{a}^{2} + \lambda_{b}^{2})\lambda_{ab} - 11\lambda_{ab}^{3}.$$
(14)

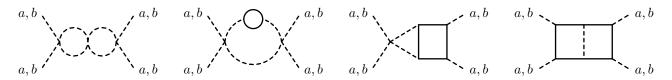


FIG. 3. Example Feynman diagrams entering the computation of the scalar four-point functions at the two-loop level relevant for extracting the renormalization constants of the quartic couplings, $\delta \lambda_{a/b/ab}$.

Anomalous dimensions for order parameters

The anomalous dimensions $\gamma_{r_{a,b}}$ control the RGEs for the order parameters, $r_{a,b}$, via

$$\gamma_{r_X} \equiv \frac{d \log r_X}{d \log \mu} = \sum_{i=1}^{\infty} \left(\frac{1}{16\pi^2}\right)^n \gamma_{r_X}^{(n)},$$
(15)

where $X \in \{a, b\}$ and with the one- and two-loop contributions

$$\gamma_{r_a}^{(1)} = 4N_{\Psi}g_a^2 + 5\lambda_a + 3\frac{r_b}{r_a}\lambda_{ab} \,, \tag{16}$$

$$\gamma_{r_a}^{(2)} = -\frac{N_{\Psi}}{2} g_a^2 \left(15 g_b^2 + 11 g_a^2 + 40 \lambda_a \right) - \frac{25}{2} \lambda_a^2 - \frac{3}{2} \lambda_{ab}^2 ,$$

$$+ \frac{r_b}{r_a} \left(N_{\Psi} g_b^2 \left(6 g_a^2 - 12 \lambda_{ab} \right) - 6 \lambda_{ab}^2 \right), \tag{17}$$

and by analogy $\gamma_{r_b} = \{\gamma_{r_a} \text{ with } a \leftrightarrow b\}$. These RGEs depend on the ratio r_b/r_a because the order parameters receive additive renormalization corrections. The sign convention in Eq. (15) implies that the scaling dimension of the bosons on the fixed points, $\theta_{r_{a,b}}$, receives the quantum correction

$$\theta_{r_{a,b}} = D_{r_{a,b}} - \gamma_{r_{a,b}}^* \,, \tag{18}$$

with $D_{r_{a,b}} = 2$ the engineering/classical dimension of the respective order parameter and $\gamma_{r_{a,b}}^*$ its anomalous dimension evaluated at the given fixed point.

Scalar anomalous dimensions

Using the field renormalization constants, $Z_{a,b}$, we can also define anomalous dimensions for the bosonic degrees of freedom a_i and b_j as

$$\gamma_X \equiv \frac{d \log Z_X}{d \log \mu} = \sum_{i=1}^{\infty} \left(\frac{1}{16\pi^2}\right)^n \gamma_X^{(n)}, \qquad (19)$$

where $X \in \{a, b\}$ and with

$$\gamma_a^{(1)} = N_{\Psi} g_a^2,$$
 (20)

$$\gamma_a^{(2)} = \frac{5}{8} \lambda_a^2 + \frac{3}{8} \lambda_{ab}^2 - \frac{7}{8} N_\Psi g_a^4 - \frac{15}{8} N_\Psi g_a^2 g_b^2 \,. \tag{21}$$

By analogy, $\gamma_b = {\gamma_a \text{ with } a \leftrightarrow b}.$

Fermion anomalous dimension

For completeness, we define here in analogy to the bosonic sector also the "fermion anomalous dimension" based on the fermion-field renormalization

$$\gamma_{\Psi} \equiv \frac{d \log Z_{\Psi}}{d \log \mu} = \sum_{i=1}^{\infty} \left(\frac{1}{16\pi^2}\right)^n \gamma_{\Psi}^{(n)}, \qquad (22)$$

where the one- and two-loop contributions read

$$\gamma_{\Psi}^{(1)} = \frac{3}{16} \left(g_a^2 + g_b^2 \right) \,, \tag{23}$$

$$\gamma_{\Psi}^{(2)} = -\frac{9}{16} N_{\Psi} \left(g_a^4 + g_b^4 \right) - \frac{9}{128} \left(g_a^2 + g_b^2 \right)^2. \tag{24}$$

In the next section, we use the β -functions and anomalous dimensions of the $d=4-\epsilon$ theory presented here to explore the RG fixed-point structure of the theory and to study the d=3 theory.

IV. FIXED POINTS AND CRITICAL BEHAVIOR

In this section, we analyze the fixed points of the β functions at the two-loop order. First, to compare to the quantum Monte Carlo (QMC) data from Ref. [39], we constrain the model to the higher-symmetric subspace in which $g_a^2 = g_b^2$, $\lambda_a = \lambda_b$, and $\lambda_{ab} = \lambda_c$. We extend the analysis to general flavor number to explore possible fixed-point collisions and recurrences along the $N_f = 4N_{\Psi}$ axis. Secondly, we explore the fixed-point structure and stability of the full model containing the five independent couplings in Eq. (1) for the graphene case, i.e., $N_f = 2$. We extend the leading-order analysis, which identified two stable fixed points, 40 to the next order in the ϵ expansion. We also present results beyond the strict fixed-order ϵ -expansion by numerically evaluating the fixed points directly from the two-loop β -functions. In this case, we find numerous fixed-point collisions as a function of ϵ .

To determine the stability of each fixed point with coordinates $c_j^* \in \{g_a^{2*}, g_b^{2*}, \lambda_a^*, \lambda_b^*, \lambda_{ab}^*\}$, we linearize the RG flow in its vicinity:

$$\beta_{c_i} = S_{ij} \left(c_j - c_j^* \right) + \mathcal{O} \left((c - c^*)^2 \right),$$
 (25)

where S_{ij} denotes the stability matrix,

$$S(\lbrace c_n \rbrace)_{ij} \equiv \frac{\partial \beta_{c_i}(\lbrace c_n \rbrace)}{\partial c_i} \Big|_{c^*}.$$
 (26)

Using the five eigenvalues of the stability matrix, we define the quantity θ_k , with $k=1,\ldots,5$, as the kth eigenvalue, multiplied by a factor of -1. In the following, we assess the stability of a fixed point based on the sign of the corresponding θ_k and will refer to the θ_k 's as the eigenvalues of the stability matrix. Specifically, a positive value of θ_k corresponds to an IR repulsive (unstable, relevant) direction, whereas a negative value corresponds to an IR attractive (stable, irrelevant) direction of the RG flow. We denote a fixed point as stable when all directions in the RG flow are IR attractive. In our analysis, the

bosonic order parameters r_a and r_b are always set to zero, as they correspond to relevant directions in the RG flow.

A. Symmetric subspace for general N_f

In the symmetric subspace relevant to the model studied by QMC, we have

$$g_a^2 = g_b^2 = g^2$$
, $\lambda_a = \lambda_b = \lambda$, $\lambda_{ab} = \lambda_c$. (27)

The β -functions at two-loop order then reduce to

$$\beta_{g^2} = -\epsilon g^2 + \frac{1}{16\pi^2} g^4 (5 + N_f) + \frac{1}{(16\pi^2)^2} g^2 \left[g^4 \left(-6N_f - \frac{49}{8} \right) - g^2 (5\lambda + 9\lambda_c) + \frac{5}{2} \lambda^2 + \frac{3}{2} \lambda_c^2 \right],$$
(28)

$$\beta_{\lambda} = -\epsilon \lambda + \frac{1}{16\pi^{2}} \left[-N_{f}g^{4} + 2N_{f}g^{2}\lambda + 11\lambda^{2} + 3\lambda_{c}^{2} \right] + \frac{1}{(16\pi^{2})^{2}} \left[8N_{f}g^{6} + N_{f}g^{4} \left(3\lambda_{c} - \frac{9}{2}\lambda \right) - N_{f}g^{2} \left(11\lambda^{2} + 3\lambda_{c}^{2} \right) - 3\left(23\lambda^{3} + 5\lambda\lambda_{c}^{2} + 4\lambda_{c}^{3} \right) \right], \tag{29}$$

$$\beta_{\lambda_c} = -\epsilon \lambda_c + \frac{1}{16\pi^2} \left[-3N_f g^4 + 2N_f g^2 \lambda_c + 2\lambda_c (5\lambda + 2\lambda_c) \right] + \frac{1}{(16\pi^2)^2} \left[16N_f g^6 + N_f g^4 \left(5\lambda - \frac{5}{2}\lambda_c \right) - 2N_f g^2 \lambda_c (5\lambda + 2\lambda_c) - \lambda_c (5\lambda + \lambda_c) (5\lambda + 11\lambda_c) \right]. \tag{30}$$

Ref. [40] showed that the one-loop level of these equations feature fixed-point solutions for $N_f < N_c^< \approx 0.0164$. Moreover, the one-loop equations also admit a fixed-point solution for $N_f > N_c^> \approx 16.83$, but not for the physically relevant case, $N_f = 2$.

To search for possible fixed points in the two-loop β functions, we first evaluate the full set of equations for fixed ϵ and for various values of N_f . This approach enables us to find new fixed points only present at the two-loop order. Hence, it differs from the strict fixed-order ϵ -expansion, where we compute perturbative corrections to one-loop fixed points. In Figure 4, we have summarized our findings. Concretely, we mark positions in the $\epsilon - N_f$ plane with a red dot, where a stable fixed-point solution of the two-loop β -functions exists. In addition, the gray regions show values of N_f , where the leading-order (LO) β functions indicate the existence of a stable fixed-point solution. Moreover, we display next-to-leading order (NLO) corrections to this critical number of fermions as blue dashed lines, which we will derive below in Eqs. (31) and (33). Notably, our numerical approach not only exposes outliers among stable solutions, e.g., $(\epsilon, N_f) \sim (0.75, 10)$, but also exhibits sharp kinks in the boundary of the stable fixed-point solutions, which would not appear in the strict ϵ -expansion. Very similar behavior can already be observed within the well-known purely bosonic case, q=0. For example, for the decoupled fixed point (DFP) where

 $\lambda_c^*=0$, the explicit solution of the NLO β -functions reads $\lambda^*=(11+\sqrt{121-276\epsilon})/552$. This becomes complex for $\epsilon\geq 121/276\approx 0.438$ and hence does not correspond to a physically admissible solution anymore. As expected, our findings agree with the LO results of Ref. [40] for small ϵ , i.e., the critical values of N_f coincide in the limit $\epsilon\to 0$, both at LO and NLO (see dashed-dotted lines in Figure 4).

We already know that to first order in ϵ , the case $N_f=2$ does not feature a fixed point, i.e., we cannot build on that at the next order in ϵ . However, using the full numerical solution, we can track whether the two-loop corrections bring the values for N_c^{\lessgtr} closer to $N_f=2$, by setting up the corresponding series in ϵ , i.e.,

$$N_c^{>} \approx 16.83 + \delta N_c^{> (2\text{-loop})} \epsilon + \mathcal{O}(\epsilon^2),$$
 (31)

where $\delta N_c^{>(2\text{-loop})}$ is to be determined, see Refs. [58] and [59]. Our setup for the numerical approximation of the slope uses a step size in ϵ of width $\Delta_{\epsilon} = 0.002$ and in the flavor number, we use 200 evenly-spaced logarithmic values in the ranges $1/2 \leq N_f \leq 50$. We start at $\epsilon_{\text{start}} = 0.002$ and determine the boundary separating stable and unstable solutions, and calculate the slope for small ϵ including points up to $\epsilon = 0.15$ using linear regression, while fixing the intercept at the one-loop result $N_c^>(\epsilon = 0) = 16.83$. We

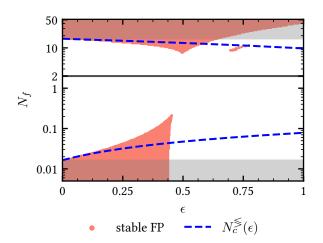


FIG. 4. The red dots mark the positions in the $\epsilon - N_f$ plane where a fixed-point (FP) solution at two-loop order exists. The gray shaded areas indicate the region in which a FP exists at one-loop order. The solid, black horizontal line shows the case $N_f = 2$ and the dashed, blue lines correspond to the extrapolation of the two-loop correction in Eqs. (31) and (33) for small ϵ .

accordingly extract $\delta N_c^{> (2\text{-loop})}$ from Figure 4 as

$$\delta N_c^{>(2\text{-loop})} \approx -7.14, \tag{32}$$

and analogously, using a different range for the flavor number, i.e., $0.0001 \le N_f \le 0.5$, determine the lower boundary

$$N_c^{<} \approx 0.0164 + \delta N_c^{< (2\text{-loop})} \epsilon + \mathcal{O}(\epsilon^2),$$
 (33)

with

$$\delta N_c^{<\,(\text{2-loop})} \approx 0.062\,. \tag{34}$$

The two lines corresponding to Eqs. (31) and (33) are depicted by the blue, dashed lines in Figure 4.

We conclude that the two-loop order brings the critical flavor number significantly closer to the physical case of $N_f = 2$. Therefore, it may still be possible that the true critical flavor number $N_{f,c}$ is close or even below $N_f = 2$, which would allow critical, or at least pseudo-critical scaling as we discuss further below.

Unconstrained parameter space for $N_f = 2$

Building upon the results of Ref. [40] and the twoloop results presented in Section III, we first evaluate the perturbative fixed points within the ϵ -expansion at two-loop accuracy. Here, we restrict the analysis to the case corresponding to graphene, and thus fix $N_f = 2$. At one-loop level, the β -functions for the Yukawa and the quartic sector decouple, allowing for an independent study of the two subsectors. This is no longer the case

at the two-loop order. The values of the couplings at the fixed points admit a perturbative expansion for small ϵ :

$$c_i^* = D_i \epsilon + F_i \epsilon^2 + \mathcal{O}(\epsilon^3), \tag{35}$$

with $c_i \in \{g_a^2, g_b^2, \lambda_a, \lambda_b, \lambda_{ab}\}$. The one-loop β -functions determine the coefficients D_i , whereas we compute F_i by solving the system of two-loop β -functions:

$$\forall i: \beta_{c_i} \left(\left\{ c_j^* \right\} \right) = 0, \tag{36}$$

where β_{c_i} is the β -function of the coupling c_i . To compactly present the fixed points, we label the fixed-point coordinates in the Yukawa sector as Y_i and in the bosonic one as B_k . The tuple formed by the two coordinates describes the fixed point: (Y_i, B_k) . We express the fixed-point couplings in terms of the rescaled couplings

$$\bar{g}_{a,b}^2 \equiv \frac{g_{a,b}^{*2}}{16\pi^2}, \qquad \bar{\lambda}_{a,b,ab} \equiv \frac{\lambda_{a,b,ab}^*}{16\pi^2},$$

introduced for brevity.

We will not discuss the already extensively studied family of purely bosonic fixed points, i.e.,

$$Y_1: \bar{g}_a^2 = 0, \ \bar{g}_b^2 = 0,$$
 (37)

in which available calculations have identified stable fixedpoint solutions at a precision beyond NLO.⁶⁰ Concretely, for $N_f = 2$ we obtain a total of four different perturbative fixed points with physical values for all couplings at $\mathcal{O}(\epsilon^2)$:

$$(Y_2, B_{1b}), (Y_2, B_{2b}), (Y_3, B_{1a}), (Y_3, B_{2a}).$$
 (38)

In terms of the rescaled couplings, the coordinates of the fixed points in Eq. (38) in the Yukawa sector read

$$Y_2: \bar{g}_a^2 = 0, \quad \bar{g}_b^2 = \frac{2}{5}\epsilon + \frac{11689}{60500}\epsilon^2,$$
 (39)

$$Y_3: \{Y_2 \text{ with } a \leftrightarrow b\},$$
 (40)

and in the bosonic sector we have $\bar{\lambda}_{ab} = 0$ and

$$B_{1a}: \bar{\lambda}_a = \frac{8}{55}\epsilon + \frac{311246}{3161125}\epsilon^2, \quad \bar{\lambda}_b = \frac{1}{11}\epsilon + \frac{69}{1331}\epsilon^2,$$
 (41)

$$B_{2a}: \bar{\lambda}_a = \frac{8}{55}\epsilon + \frac{311246}{3161125}\epsilon^2, \quad \bar{\lambda}_b = 0,$$
 (42)

$$B_{1b}: \{B_{1a} \text{ with } a \leftrightarrow b\},$$
 (43)

$$B_{2b}: \{B_{2a} \text{ with } a \leftrightarrow b\}.$$
 (44)

We find by explicit computation that further fixedpoint solutions associated to the Yukawa sector $Y_4: \bar{g}_a^2 =$ $\bar{g}_b^2 \neq 0$ have complex solutions for the quartic couplings: $\bar{\lambda}_{a/b/ab} \notin \mathbb{R}$. Since these fixed points do not constitute physical solutions, we do not include them in the following discussion. We note, however, that the existence of physical and stable solutions does depend on the number

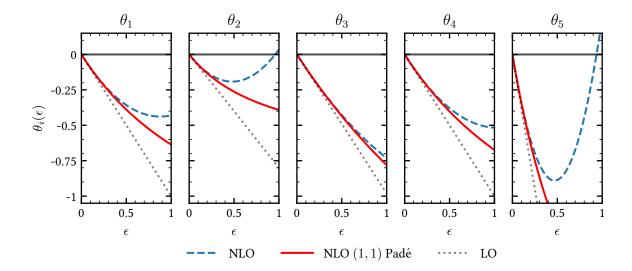


FIG. 5. The five eigenvalues of the stability matrix in Eq. (26) multiplied by a factor of -1, i.e., θ_k , as a function of ϵ , evaluated at the decoupled fixed points (Y_2, B_{1b}) or equivalently (Y_3, B_{1a}) . The gray dotted, blue dashed, and solid red lines correspond to the LO, NLO, and NLO (m = 1, n = 1)-Padé results, respectively. Taking the limit $\epsilon \to 1$, two of the θ_k 's become positive at NLO, making the fixed point unstable (IR repulsive). Considering, however, the NLO Padé approximant, the fixed points retain their stability at two-loop order.

of fermions, N_f . This is apparent also from our previous discussion of the symmetric subsystem in which we extrapolated the critical number of fermions in the 3d case to $N_{f,c}^<(\epsilon=1)\approx 0.0784$ and $N_{f,c}^>(\epsilon=1)\approx 9.69$, cf., Eqs. (31) and (33).

The one-loop fixed-point analysis on Ref. [40] showed that the two fixed points

$$(Y_2, B_{1b}), (Y_3, B_{1a}),$$
 (45)

were the only stable ones in the physical 3d case, obtained by taking the limit $\epsilon \to 1$. As all fixed points of the system, they are symmetric with respect to exchanging the labels $a \leftrightarrow b$ in all the couplings. Given that the mixed quartic coupling, λ_{ab} , is zero at these fixed points, they are commonly denoted as DFPs.

When including the two-loop corrections, we see that up to second order in the ϵ -expansion, two of the five eigenvalues of the stability matrix become positive close to d = 3, see Figure 5, making the one-loop-stable fixed points in Eq. (45) unstable. Considering, however, the (m=1, n=1) Padé approximant (the m=0, n=2 one is divergent), all five eigenvalues stay negative, indicating that the two fixed points retain their one-loop stability even in the physical case of $\epsilon \to 1$. In Appendix B we provide the full expression for the five eigenvalues of the stability matrix for all fixed points in Eq. (38) up to $\mathcal{O}(\epsilon^2)$. We thus find that in the 3d limit there are no further stable fixed points beyond the one-loop ones after including the two-loop corrections. In Figure 5, we show the five eigenvalues of the two candidate stable fixed points as a function of ϵ at LO, NLO, and NLO (1,1)-Padé. We see that all eigenvalues are negative as $\epsilon \to 1$ at NLO (1,1)-Padé (red solid lines).

A further check of our computation is provided by Aharony's exact scaling relation⁶¹

$$\theta_{ab} = \frac{1}{\nu_a} + \frac{1}{\nu_b} - d\,, (46)$$

which relates the critical exponents ν_a of the 3d Heisenberg universality class and ν_b of the chiral Heisenberg universality class, 33,40 to the scaling dimension θ_{ab} of the mixed quartic coupling λ_{ab} , evaluated at the DFPs in Eq. (45). Using the anomalous dimensions of the order parameters $a_i t_i$ and $b_j t_j$, as given in Eq. (15), we can determine the critical exponents $\nu_{a,b}$ at the DFPs. Our conventions imply that

$$\frac{1}{\nu_{a,b}} = D_{r_{a,b}} - \gamma_{r_{a,b}}^* \,, \tag{47}$$

with $D_{r_a} = 2$ the engineering/classical dimension of the respective order parameter and $\gamma_{r_{a,b}}^*$ the value of the anomalous dimension evaluated on the (decoupled) fixed point. The one-loop result for the critical exponents of the (chiral) Heisenberg universality class are in agreement with the discussion in Ref. [40]. Including the two-loop contribution we find

$$\frac{1}{\nu_a} = 2 - \frac{5}{11}\epsilon - \frac{415}{2662}\epsilon^2 + \mathcal{O}(\epsilon^3), \tag{48}$$

and analogously for the critical exponent of the chiral Heisenberg universality class:

$$\frac{1}{\nu_b} = 2 - \frac{84}{55}\epsilon + \frac{2576729}{6322250}\epsilon^2 + \mathcal{O}(\epsilon^3), \qquad (49)$$

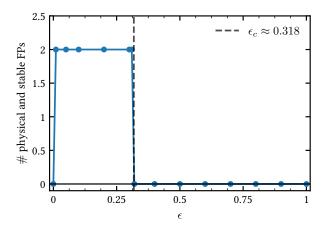


FIG. 6. The number of stable fixed points (FPs) with a physical value of all couplings, i.e., $\forall i: c_i^* \geq 0$, as a function of ϵ , found by the numerical solution of the corresponding β -functions. For small ϵ , the ϵ -expansion predicts two stable FPs, cf., Eq. (45). For $\epsilon = 0$, the system exhibits no stable FP, as both perturbative FPs coincide with the unstable Gaussian FP. The blue dots mark the values of ϵ , for which we performed the numerical study. At a critical value of ϵ , i.e., $\epsilon_c \approx 0.318$, we observe that the two stable FPs lose their stability by colliding with new FPs that are only present at two-loop order. After crossing the critical threshold ϵ_c , the system exhibits no stable, physical FPs, in particular not in the 3d case, obtained by taking the limit $\epsilon \to 1$. This result retains higher-order terms in ϵ and appears to be in tension with the previous findings using the strict ϵ -expansion predictions (cf. Figure 5), whose NLO (1,1) Padé approximant predicted the existence of two physical and stable 3d FPs.

which are in agreement with the literature. ^{33,62,63} Using Aharony's scaling relation in Eq. (46) and $d = 4 - \epsilon$, we find

$$\theta_3 = \theta_{ab} = -\frac{54}{55}\epsilon + \frac{795552}{3161125}\epsilon^2 + \mathcal{O}(\epsilon^3),$$
 (50)

which corresponds to the NLO eigenvalue θ_3 (cf. Figure 5 and Appendix B). The scaling dimension θ_{ab} becomes negative in the limit $\epsilon \to 1$, which indicates that the coupling λ_{ab} is irrelevant at two-loop order, thus supporting the stability of the Heisenberg+chiral Heisenberg fixed point, as indicated by beyond NLO calculations, cf. Ref. 40.

We conclude that the perturbative ϵ -expansion ansatz does not unambiguously settle the stability of the fixed points in the physically relevant 3d case. Specifically, expanding the eigenvalues of all the perturbative fixed points in Eq. (38) at NLO shows that the one-loop-stable fixed points in Eq. (45) lose their stability at $\epsilon \approx 0.95$ and that the system exhibits no stable perturbative fixed point in the 3d case after taking $\epsilon \to 1$. Making use, however, of the (1,1) NLO Padé approximant, the two fixed points do retain their one-loop stability.

We close this section with a brief numerical study of the fixed-point solutions of the β -functions that goes beyond the strict $\epsilon \to 0$ limit. To this end, we vary $\epsilon \in [0, 1.0]$;

for small values of ϵ we expect good agreement with the perturbative expansion. A thorough analysis shows that, starting from $\epsilon > 0$, the perturbative, stable fixed-point candidates in Eq. (45) remain stable, until they collide with two new non-perturbative and unstable fixed points only present at two-loops at a critical $\epsilon_c \approx 0.318$. After crossing this critical threshold, no stable fixed point exists, in particular not in the 3d case. For $\epsilon = 0$, the system exhibits no stable fixed point, as both perturbative fixed points coincide with the unstable Gaussian one. We have summarized our non-perturbative findings in Figure 6, where we show the dependence of the amount of stable fixed points with physical values for all the couplings, i.e., $\forall i: c_i \geq 0$, against ϵ .

These findings are thus in agreement with the NLO prediction from the two-loop β -functions using the strict ϵ -expansion but are in tension with the corresponding NLO (1, 1)-Padé (see Figure 5), which states that the one-loop-stable fixed points in Eq. (45) retain their stability at two-loops even in the physical 3d case, i.e., taking the limit $\epsilon \to 1$.

V. DISCUSSION

In summary, we have investigated a Gross-Neveu-Yukawa field theory describing a number of N_f Dirac fermions coupled to two triplets of SO(3) order parameters, employing the perturbative renormalization group at two-loop level in $4 - \epsilon$ dimensions. The study was motivated by the recent numerical observation of relativistic quantum criticality, employing large-scale quantum Monte Carlo simulations.³⁹ This criticality was found to be in conflict with the absence of a stable renormalization-group fixed point of the above Gross-Neveu-Yukawa theory for the physically relevant number of Dirac fermions, i.e., $N_f = 2$. In fact, at the one-loop level a stable fixed point only appears in the field theory for large, $N_f > N_c^> \approx 16.8$ or very small $N_f < N_c^{<} \approx 0.0164$. For the intermediate range $N_f \in [N_c^{<}, N_c^{>}]$, the fixed point disappears into the complex plane due to a fixed-point collision and annihilation. 58,62,64-77 In the present work, we investigated both the symmetric subspace studied by quantum Monte Carlo simulations and the full, unconstrained parameter space of the model. In the unconstrained parameter space, we found a pair of stable fixed points at NLO (1, 1)-Padé, which are, however, not part of the symmetric subsystem.

For the symmetric subsystem, a key result of our present renormalization-group study at two-loop order is the ϵ correction to the upper and lower critical flavor numbers, i.e., N_c^{\lessgtr} . Both corrections drive the critical flavor numbers closer to the physical case $N_f=2$ with respect to the one-loop result. However, the magnitude of the corrections as $\epsilon \to 1$ is not large enough to make the fixed points stable for the physical system, which thus still suggests the absence of criticality in 2+1 dimensions.

Hence, our two-loop study cannot fully resolve the conflicting findings between the quantum Monte Carlo data and the field-theoretical approach. Still, the two-loop corrections do point towards the possibility that the renormalization-group fixed point might be restored at even higher-loop orders, e.g., by further suppressing the value of $N_c^>$ towards $N_f=2$, similar to what is observed in the abelian Higgs model at four loops.⁵⁸

We note that even the case of, e.g., $N_c^> \gtrsim 2$, would be very interesting, because it could naturally explain the observation of approximate power laws and a large correlation length, reminiscent of critical behavior, despite the absence of true criticality. Such behavior could occur due to pseudo-critical walking and Miransky scaling, appearing when the renormalization-group flow is governed by an underlying complex conformal field theory (CFT). ^{76,78}

A complex CFT is the natural consequence of a fixed-point collision and annihilation as observed in our study and is expected to be a common phenomenon in many physical systems. ⁷⁸ However, a numerical confirmation is inherently difficult due to the similarity of continuous and very weak first-order behavior in a finite-size system. A distinct detection tool for future quantum Monte Carlo studies could be the analysis of the entanglement entropy as, e.g., pushed forward recently in the context of deconfined quantum phase transitions. ^{79,80}

For future field-theoretical studies, it could be very interesting to extract even higher-order corrections to the critical number of fermion flavors in order to consolidate or refute such complex CFT scenario.

Acknowledgments

We thank L. Di Pietro for stimulating discussions. MMS acknowledges funding from the Deutsche Forschungsgemeinschaft (DFG, German Research Foundation) within Project-ID 277146847, SFB 1238 (project C02), and the DFG Heisenberg programme (Project-ID 452976698). MU acknowledges support by the Erasmus+ programme of the European Union and is grateful to, both the University of Trieste and the ICTP for the kind hospitality during the preparation of this work. IFH is supported by the NSERC of Canada.

Appendix A: Continuation from d = 3 to d = 4

In this section, we continue the Euclidean d=3 Lagrangian in Eq. (1) to $d=4-\epsilon$ dimensions. For convenience, we also make the transition to Minkowskian spacetime since all our computations are performed in it. We start in d=3-dimensional Euclidean spacetime, where Dirac fermions are described by complex two-component spinors and furthermore add a label "E" to indicate when the objects are in Euclidean spacetime. Since bosons continue trivially into higher dimensions, we focus on the fermion sectors, i.e., $\mathcal{L}_{\psi}^{\rm E}$ and $\mathcal{L}_{\psi ab}^{\rm E}$.

The tensor product in the Lagrangian in Eq. (1)

$$M_1 \otimes M_2 \otimes M_3$$
, (A1)

with M_1, M_2, M_3 being 2×2 matrices, acts upon the two valley, two sublattice, and two spin degrees of freedom of the eight-component fermion field ψ , cf., Ref. [40]. We rewrite this tensor notation by rearranging the eight components of ψ into the two components of a complex Dirac fermion in d=3 that is a bidoublet of $SU(2)_A \times SU(2)_B$:

$$\psi \longrightarrow \Psi_{\alpha,aA}^{d=3}$$
. (A2)

Here, Greek letters ($\alpha=1,2$) denote the spin components, which will end up being the Lorentz spinor indices, lower-case Latin letters (a=1,2) are the fundamental indices of SU(2)_A (valley degrees of freedom), and uppercase Latin letters (A=1,2) are the fundamental indices of SU(2)_B (sublattice degrees of freedom). Lowered SU(2)_{A/B} indices are always assumed to be in the fundamental representation of SU(2) (as in Eq. (A2)), whereas raised ones denote indices in the anti-fundamental representation. By contracting with ϵ^{ab} or ϵ^{AB} we can raise (or lower) SU(2) indices to relate the fundamental and anti-fundamental representations.

We reserve the letters i, j = 1, 2, 3 to be used as adjoint indices of $SU(2)_{A/B}$. The order parameters transform in the adjoint representation of their respective SU(2), which can be obtained from the traceless part of the $\mathbf{2} \otimes \overline{\mathbf{2}}$ tensor product. Therefore, to construct invariants, it is useful to express the order parameters as

$$(a_i t_i)_a^b$$
, $(b_j t_j)_A^B$, (A3)

with $t_i = \sigma_i/2$.

Finally, we define the conjugate field $\Psi^{\dagger} \equiv \overline{\Psi}\beta \equiv \overline{\Psi}\gamma_{\rm E}^0$ with $\beta^2 = \sigma_3^2 = \mathbb{1}_2$ to find by rewriting Eq. (1):

$$\mathcal{L}_{\Psi}^{E} = \overline{\Psi}_{aA}^{d=3} \left[\partial_{E} \epsilon^{ab} \epsilon^{AB} \right] \Psi_{bB}^{d=3} , \qquad (A4)$$

$$\mathcal{L}_{\Psi ab}^{E} = -\overline{\Psi}_{aA}^{d=3} \left[g_{a} \left(a_{i} t_{i} \right)^{ab} \epsilon^{AB} + g_{b} \epsilon^{ab} \left(b_{j} t_{j} \right)^{AB} \right] \Psi_{bB}^{d=3} ,$$

where we have suppressed the spinor indices. Here, we identified the d=3 gamma matrices in Euclidean spacetime as $\{\gamma_{\rm E}^0, \gamma_{\rm E}^1, \gamma_{\rm E}^2\} \equiv \{\beta, -i\beta\sigma_1, -i\beta\sigma_2\}$, which satisfy the Clifford algebra $\{\gamma_{\rm E}^\mu, \gamma_{\rm E}^\nu\} = 2\delta^{\mu\nu}$.

The transition from Euclidean to Minkowskian spacetime is thereafter straightforward by performing a Wick rotation, i.e., rotating the Euclidean time, τ , to the Minkowskian time, $t\colon t\to -i\tau$. This rotation implies replacing $\partial_{\rm E}\to i\partial_{\mu}\gamma^{\mu}$, where γ^{μ} denotes the gamma matrices in Minkowskian spacetime, which satisfy $\{\gamma^{\mu},\gamma^{\nu}\}=2g^{\mu\nu}$ with $g^{\mu\nu}={\rm diag}(+,-,-)$. Concretely, the gamma matrices in Minkowskian spacetime are related to their Euclidean counterparts via $\gamma^0\to\gamma^0_{\rm E}=\beta$ and $\gamma^k\to -i\gamma^k_{\rm E}=-\beta\sigma^k$ for k=1,2. Thus, we rewrote the original Euclidean d=3 Lagrangian with an eight-component complex fermion field ψ into a Lagrangian in Minkowskian spacetime, featuring a

single two-component complex Dirac fermion that transforms as a bidoublet under the global symmetry group $SU(2)_A \times SU(2)_B$.

Next we derive our continuation of the d=3 Lagrangian to $d=4-\epsilon$ dimensions. Our Dirac fermions in d=3 are two-component complex spinors, whereas d=4 Dirac fermions are complex, four-component spinors or equivalently two, complex two-component Weyl spinors. Therefore, naïvely we expect that the continuation will double the fermionic degrees of freedom. We shall see that this is indeed the case if we couple the fermions to adjoint order parameters.

The attempt to derive a continuation without doubling the fermionic degrees of freedom by interpreting the d=3 two-component Dirac field, $\Psi_{aA}^{d=3}$, as a corresponding two-component Weyl field in d = 4, ξ_{aA} , is not possible. The reason is twofold: i) for ξ_{aA} there is no Lorentz-invariant counterpart to the d=3 Yukawa term, e.g., $\overline{\Psi}^{d=3}(a_it_i)\Psi^{d=3}$, since in four Minkowskian spacetime dimensions, the representation of the Lorentz group is complex, which is not the case in d=3. Thus, while complex conjugation in d=3 gives rise to an equivalent representation—allowing for Dirac mass terms—it leads to a nonequivalent representation in d=4, i.e., there is no notion of chirality in d=3. ii) there is a Lorentz-variant way to couple ξ_{aA} with adjoint order parameters. However, this contraction vanishes due to the global symmetry structure:

$$\xi_{aA}(a_i t_i)^{ab} \epsilon^{AB} \xi_{bB} = 0, \qquad (A5)$$

(analogously for $(b_j t_j)^{AB}$), which evaluates to zero due to the fact that $(a_i t_i)^{ab}$ is symmetric in the indices a and b and ξ_{aA} is an anticommuting field.

Importantly, the analogous contraction with two independent Weyl fields, ξ_{aA} and η_{aA} does not vanish, e.g.,

$$\xi_{aA}(a_i t_i)^{ab} \epsilon^{AB} \eta_{bB} \neq 0, \tag{A6}$$

and analogously for $(b_j t_j)^{AB}$. Thus, to construct a non-vanishing Yukawa interaction using Weyl fields in d=4 we have to *double* the fermionic degrees of freedom with respect to d=3, i.e., we need two *different flavors* of Weyl fields.

In fact, the form of Eq. (A6) is precisely the one we obtain when we decompose the reducible, complex Dirac field, $\Psi^{d=3}_{aA}$ in its irreducible, real two-component Majorana fields:

$$\Psi_{aA}^{d=3} = \chi_{1,aA} + i \,\chi_{2,aA} \,. \tag{A7}$$

In terms of χ_1 and χ_2 , the Yukawa terms read

$$\begin{split} \overline{\Psi}_{aA}^{d=3}(a_it_i)^{ab}\epsilon^{AB}\Psi_{bB}^{d=3} &= i\overline{\chi}_{1,aA}(a_it_i)^{ab}\epsilon^{AB}\chi_{2,bB} \\ &- i\overline{\chi}_{2,aA}\underbrace{(a_it_i)^{ab}\epsilon^{AB}}_{=-(a_it_i)^{ba}\epsilon^{BA}}\chi_{1,bB} \\ &= 2i\overline{\chi}_{1,aA}(a_it_i)^{ab}\epsilon^{AB}\chi_{2,bB} \neq 0 \,, \end{split}$$

TABLE II. Field content of $4 - \epsilon$ dimensional theory in Eq. (A10) and its transformation properties under the global $SU(2)_A \times SU(2)_B$ symmetry and the Lorentz group. n labels the number of Dirac-bidoublet fermions.

	$SU(2)_A$	$SU(2)_B$	Lorentz
$\eta_{n,aA},\xi_{n,aA}$	2	2	(1/2,0)
$\Psi_{n,aA}$	2	2	(1/2,0) + (0,1/2)
a_i	3	_	-
b_j	_	3	_

and analogously for $(b_j t_j)^{AB}$. This illustrates why doubling the fermionic degrees appears to be the natural way to continue the theory via Eq. (A6).

Going back to the d=4 description we can bundle together the two different flavors of Weyl fields, ξ_{aA} and η_{aA} —taken without loss of generality to transform under the left-chiral representation (1/2,0) of Lorentz—into one four-component Dirac field, Ψ_{aA} , as

$$\Psi_{aA} \equiv \begin{pmatrix} \eta_{\alpha,aA} \\ \xi_{aA}^{\dagger \dot{\alpha}} \end{pmatrix} , \qquad \overline{\Psi}^{aA} = \left(\xi^{\alpha,aA}, \eta_{\dot{\alpha}}^{\dagger aA} \right) . \quad (A9)$$

Here, α denotes the spinor index for left-chiral spinors and $\dot{\alpha}$ denotes the right-chiral (0,1/2) one.

The final step to fix the continuation is to ensure that we describe the correct number of fermionic degrees of freedom, when we extrapolate the $d=4-\epsilon$ results to d=3. This is not possible with a single Ψ_{aA} . We achieve this instead by introducing N_{Ψ} number of Diracbidoublet fermions, $\Psi_{n,aA}$. To describe the original eight independent fermionic components of graphene in d=3, i.e., $N_f=2$ four-component fermion fields corresponding to a single $\Psi_{aA}^{d=3}$, within the ϵ -expansion, we must set $N_{\Psi}=1/2$. For the definition of N_f from Ref. [40], this corresponds to $N_f=4N_{\Psi}$. In terms of $\Psi_{n,aA}$ the resulting, manifestly Lorentz-invariant Lagrangian in $d=4-\epsilon$ reads:

$$\mathcal{L} = \overline{\Psi}_{n} i \partial \Psi_{n} + \frac{1}{2} \left[(\partial_{\mu} a_{i}) \left(\partial^{\mu} a_{i} \right) + (\partial_{\mu} b_{j}) \left(\partial^{\mu} b_{j} \right) \right]$$

$$- \frac{r_{a}}{2} (a_{i} a_{i}) - \frac{r_{b}}{2} (b_{j} b_{j})$$

$$- \frac{\lambda_{a}}{8} (a_{i} a_{i})^{2} - \frac{\lambda_{b}}{8} (b_{j} b_{j})^{2} - \frac{\lambda_{ab}}{4} (a_{i} a_{i}) (b_{j} b_{j})$$

$$- g_{a} \overline{\Psi}_{n} (a_{i} t_{i}) \Psi_{n} - g_{b} \overline{\Psi}_{n} (b_{j} t_{j}) \Psi_{n} ,$$

$$(A10)$$

where for brevity we have kept all Lorentz and $SU(2)_{A/B}$ contractions implicit. In Table II we summarize the transformation properties of all fields under the Lorentz group and the global symmetry $SU(2)_A \times SU(2)_B$.

Notice that the structure of the d=4 Lagrangian in terms of four-component Dirac fermions, Eq. (A10), is in total analogy to the Minkowskian version of the d=3 Lagrangian written in terms of two-component Dirac fermions, Eq. (A4).

Appendix B: Eigenvalues of the stability matrix within the ϵ -expansion

In this section, we provide the explicit results for all the eigenvalues of the stability matrix in Eq. (26) multiplied by a factor of -1 and denoted by θ_k for the four perturbative fixed points of Eq. (38) at NLO.

As discussed in Section IVB, taking the limit of $\epsilon \to 1$ to obtain the 3d case yields no stable fixed-point solutions, which corresponds to having at least one positive eigenvalue (IR repulsive).

Explicitly, the eigenvalues $\{\theta_1, \theta_2, \theta_3, \theta_4, \theta_5\}$ up to $\mathcal{O}(\epsilon^2)$ in $d = 4 - \epsilon$ read:

$$(Y_2, B_{1b}) \& (Y_3, B_{1a}) : \left\{ \epsilon - \frac{69\epsilon^2}{121}, \frac{4\epsilon}{5} - \frac{1148\epsilon^2}{1375}, \frac{54\epsilon}{55} - \frac{795552\epsilon^2}{3161125}, \epsilon - \frac{11689\epsilon^2}{24200}, \frac{19\epsilon}{5} - \frac{1165427\epsilon^2}{287375} \right\}, \tag{B1}$$

$$(Y_{2}, B_{1b}) & (Y_{3}, B_{1a}) : \left\{ \epsilon - \frac{69\epsilon^{2}}{121}, \frac{4\epsilon}{5} - \frac{1148\epsilon^{2}}{1375}, \frac{54\epsilon}{55} - \frac{795552\epsilon^{2}}{3161125}, \epsilon - \frac{11689\epsilon^{2}}{24200}, \frac{19\epsilon}{5} - \frac{1165427\epsilon^{2}}{287375} \right\},$$

$$(Y_{2}, B_{2b}) & (Y_{3}, B_{2a}) : \left\{ -\epsilon, \frac{4\epsilon}{5} - \frac{25881\epsilon^{2}}{30250}, \frac{29\epsilon}{55} - \frac{2576729\epsilon^{2}}{6322250}, \epsilon - \frac{11689\epsilon^{2}}{24200}, \frac{19\epsilon}{5} - \frac{1165427\epsilon^{2}}{287375} \right\}.$$
(B2)

Using the NLO eigenvalues, we can furthermore calculate (m, n) Padé approximants

$$\theta(\epsilon) = \frac{\sum_{j=0}^{m} D_j \epsilon^j}{1 + \sum_{k=0}^{n} F_k \epsilon^k}.$$
 (B3)

Since the m=0, n=2 Padé approximant diverges, the only non-trivial one to consider is the m=n=1 approximant. As a result, we find that only for the two fixed points (Y_2, B_{1b}) and (Y_3, B_{1a}) all eigenvalues stay negative (IR attractive), in particular in the (2+1)-dimensional case, indicating that these fixed points retain their LO stability.

- ¹ I. F. Herbut, Phys. Rev. Lett. **97**, 146401 (2006).
- ² I. F. Herbut, V. Juričić, and B. Roy, Physical Review B **79** (2009), 10.1103/physrevb.79.085116.
- ³ R. Boyack, H. Yerzhakov, and J. Maciejko, Eur. Phys. J. ST **230**, 979 (2021).
- ⁴ I. F. Herbut, arXiv preprint arXiv:2304.07654 (2023).
- ⁵ O. Vafek and A. Vishwanath, Annual Review of Condensed Matter Physics 5, 83 (2014).
- ⁶ T. Wehling, A. Black-Schaffer, and A. Balatsky, Advances in Physics 63, 1 (2014).
- ⁷ L. Fritz, Phys. Rev. B **83**, 035125 (2011).
- ⁸ B. Roy, V. Juričić, and I. F. Herbut, Phys. Rev. B 87, 041401 (2013).
- ⁹ L. Janssen and I. F. Herbut, Phys. Rev. B **89**, 205403
- ¹⁰ B. Knorr, Phys. Rev. B **94**, 245102 (2016).
- ¹¹ M. M. Scherer and I. F. Herbut, Phys. Rev. B **94**, 205136
- ¹² S. Hesselmann and S. Wessel, Phys. Rev. B **93**, 155157 (2016).
- ¹³ Z.-X. Li, Y.-F. Jiang, S.-K. Jian, and H. Yao, Nature communications 8, 314 (2017).
- ¹⁴ L. Classen, I. F. Herbut, and M. M. Scherer, Phys. Rev. B 96, 115132 (2017).
- ¹⁵ K. Wamer and I. Affleck, Phys. Rev. B **98**, 245120 (2018).
- ¹⁶ J. A. Gracey, Phys. Rev. D **97**, 105009 (2018).
- S. Yin, S.-K. Jian, and H. Yao, Phys. Rev. Lett. 120, 215702 (2018).
- ¹⁸ Y. Liu, Z. Y. Meng, and S. Yin, Phys. Rev. B **103**, 075147
- ¹⁹ H. Yerzhakov and J. Maciejko, Nucl. Phys. B **962**, 115241
- ²⁰ S. Ray, B. Ihrig, D. Kruti, J. A. Gracey, M. M. Scherer,

- and L. Janssen, Phys. Rev. B 103, 155160 (2021).
- X. Lu, P. Stepanov, W. Yang, M. Xie, M. A. Aamir, I. Das, C. Urgell, K. Watanabe, T. Taniguchi, G. Zhang, et al., Nature **574**, 653 (2019).
- ²² P. Stepanov, I. Das, X. Lu, A. Fahimniya, K. Watanabe, T. Taniguchi, F. H. Koppens, J. Lischner, L. Levitov, and D. K. Efetov, Nature **583**, 375 (2020).
- Y. Da Liao, Z. Y. Meng, and X. Y. Xu, Phys. Rev. Lett. **123**, 157601 (2019).
- ²⁴ N. Parthenios and L. Classen, arXivarXiv:2305.06949 (2023).
- L. Iliesiu, F. Kos, D. Poland, S. S. Pufu, D. Simmons-Duffin, and R. Yacoby, JHEP 03, 120 (2016).
- L. Iliesiu, F. Kos, D. Poland, S. S. Pufu, and D. Simmons-Duffin, JHEP **01**, 036 (2018).
- R. S. Erramilli, L. V. Iliesiu, P. Kravchuk, A. Liu, D. Poland, and D. Simmons-Duffin, Journal of High Energy Physics **2023**, 1 (2023).
- S. Chandrasekharan and A. Li, Phys. Rev. D 88, 021701 (2013).
- Y. Liu, W. Wang, K. Sun, and Z. Y. Meng, Phys. Rev. B **101**, 064308 (2020).
- ³⁰ T.-T. Wang and Z. Y. Meng, (2023), arXiv:2304.00034 [cond-mat.str-el].
- B. Ihrig, L. N. Mihaila, and M. M. Scherer, Phys. Rev. B **98**, 125109 (2018).
- L. N. Mihaila, N. Zerf, B. Ihrig, I. F. Herbut, and M. M. Scherer, Phys. Rev. B 96, 165133 (2017).
- ³³ N. Zerf, L. N. Mihaila, P. Marquard, I. F. Herbut, and M. M. Scherer, Phys. Rev. D 96, 096010 (2017).
- ³⁴ F. F. Assaad and I. F. Herbut, Phys. Rev. X 3, 031010
- ³⁵ F. Parisen Toldin, M. Hohenadler, F. F. Assaad, and I. F.

- Herbut, Phys. Rev. B 91, 165108 (2015).
- ³⁶ Y. Otsuka, S. Yunoki, and S. Sorella, Phys. Rev. X 6, 011029 (2016).
- ³⁷ J. Ostmeyer, E. Berkowitz, S. Krieg, T. A. Lähde, T. Luu, and C. Urbach, Phys. Rev. B **102**, 245105 (2020).
- ³⁸ Y. Otsuka, K. Seki, S. Sorella, and S. Yunoki, Phys. Rev. B **102**, 235105 (2020).
- ³⁹ H. Liu, E. Huffman, S. Chandrasekharan, and R. K. Kaul, Phys. Rev. Lett. **128**, 117202 (2022).
- ⁴⁰ I. F. Herbut and M. M. Scherer, Phys. Rev. B **106**, 115136 (2022).
- ⁴¹ T. Senthil, L. Balents, S. Sachdev, A. Vishwanath, and M. P. A. Fisher, Phys. Rev. B **70**, 144407 (2004).
- ⁴² A. W. Sandvik, Phys. Rev. Lett. **98**, 227202 (2007)
- ⁴³ A. Nahum, J. T. Chalker, P. Serna, M. Ortuño, and A. M. Somoza, Phys. Rev. X 5, 041048 (2015).
- ⁴⁴ T. Senthil, "Deconfined quantum critical points: a review," (2023), arXiv:2306.12638 [cond-mat.str-el].
- ⁴⁵ A. A. Belavin and A. A. Migdal, Pisma Zh. Eksp. Teor. Fiz. 19, 317 (1974).
- ⁴⁶ W. E. Caswell, Phys. Rev. Lett. **33**, 244 (1974).
- ⁴⁷ T. Banks and A. Zaks, Nucl. Phys. B **196**, 189 (1982).
- ⁴⁸ Since Eq. (3) is in Euclidean 2+1 spacetime dimensions $\partial_{\mu}\partial^{\mu} = \partial_{\tau}^2 + \partial_x^2 + \partial_y^2$.
- ⁴⁹ K. G. Wilson and J. Kogut, Physics Reports **12**, 75 (1974).
- ⁵⁰ D. M. Capper and G. Leibbrandt, Journal of Mathematical Physics 15, 86 (1974).
- ⁵¹ K. Chetyrkin, M. Misiak, and M. Münz, Nuclear Physics B **518**, 473 (1998).
- 52 In this context, we refer to "tadpole" diagrams as diagrams in which the propagators do not depend on the external momenta due to the expansion.
- ⁵³ C. Bobeth, M. Misiak, and J. Urban, Nucl. Phys. **B574**, 291 (2000).
- ⁵⁴ J. Brod, E. Stamou, and T. Steudtner, to be published (2023)
- ⁵⁵ S. Borowka, G. Heinrich, S. Jahn, S. P. Jones, M. Kerner, and J. Schlenk, Journal of Physics: Conference Series 920, 012003 (2017).
- J. Kuipers, T. Ueda, J. A. M. Vermaseren, and J. Vollinga, Comput. Phys. Commun. 184, 1453 (2013).
- ⁵⁷ D. F. Litim and T. Steudtner, Computer Physics Communications 265, 108021 (2021).
- ⁵⁸ B. Ihrig, N. Zerf, P. Marquard, I. F. Herbut, and M. M.

- Scherer, Phys. Rev. B 100, 134507 (2019).
- ⁵⁹ I. F. Herbut and Z. Tešanović, Phys. Rev. Lett. **78**, 980 (1997).
- ⁶⁰ P. Calabrese, A. Pelissetto, and E. Vicari, Phys. Rev. B 67, 054505 (2003).
- ⁶¹ A. Aharony, Phys. Rev. Lett. **88**, 059703 (2002).
- ⁶² I. Herbut, A modern approach to critical phenomena (Cambridge University Press, 2007).
- ⁶³ K. Ladovrechis, S. Ray, T. Meng, and L. Janssen, Phys. Rev. B **107**, 035151 (2023).
- ⁶⁴ A. F. Faedo, C. Hoyos, D. Mateos, and J. G. Subils, Phys. Rev. Lett. **124**, 161601 (2020).
- ⁶⁵ J. A. Gracey, I. F. Herbut, and D. Roscher, Phys. Rev. D 98, 096014 (2018).
- ⁶⁶ B. I. Halperin, T. C. Lubensky, and S.-k. Ma, Phys. Rev. Lett. **32**, 292 (1974).
- ⁶⁷ M. Nauenberg and D. J. Scalapino, Phys. Rev. Lett. **44**, 837 (1980).
- ⁶⁸ I. F. Herbut and Z. Tešanović, Phys. Rev. Lett. **76**, 4588 (1996).
- ⁶⁹ K.-I. Kubota and H. Terao, Progress of Theoretical Physics 105, 809 (2001).
- ⁷⁰ K. Kaveh and I. F. Herbut, Phys. Rev. B **71**, 184519 (2005).
- 71 H. Gies and J. Jaeckel, The European Physical Journal C -Particles and Fields 46, 433 (2006).
- ⁷² D. B. Kaplan, J.-W. Lee, D. T. Son, and M. A. Stephanov, Phys. Rev. D **80**, 125005 (2009).
- ⁷³ I. F. Herbut and L. Janssen, Phys. Rev. Lett. **113**, 106401 (2014).
- ⁷⁴ I. F. Herbut, Phys. Rev. D **94**, 025036 (2016).
- ⁷⁵ L. Janssen and I. F. Herbut, Phys. Rev. B **95**, 075101 (2017).
- ⁷⁶ V. Gorbenko, S. Rychkov, and B. Zan, J. High Energy Phys. **2018**, 108 (2018).
- ⁷⁷ V. Gorbenko, S. Rychkov, and B. Zan, SciPost Physics 5 (2018), 10.21468/scipostphys.5.5.050.
- ⁷⁸ D. B. Kaplan, J.-W. Lee, D. T. Son, and M. A. Stephanov, Phys. Rev. D **80**, 125005 (2009).
- ⁷⁹ J. Zhao, Y.-C. Wang, Z. Yan, M. Cheng, and Z. Y. Meng, Phys. Rev. Lett. **128**, 010601 (2022).
- ⁸⁰ M. Song, J. Zhao, L. Janssen, M. M. Scherer, and Z. Y. Meng, (2023), arXiv:2307.02547 [cond-mat.str-el].